Regular Article - Theoretical Physics

Quasi-Dirac neutrinos and solar neutrino data

F. Rossi-Torres[1,a], A.C.B. Machado[2,b], V. Pleitez[1,c]

[1]Instituto de Física Teórica, Universidade Estadual Paulista, R. Dr. Bento Teobaldo Ferraz 271, Barra Funda, São Paulo, SP 01140-070, Brazil
[2]Centro de Ciências Naturais e Humanas, Universidade Federal do ABC, Santo André, SP 09210-170, Brazil

Abstract We will present an analysis of the solar neutrino data in the context of a $3 + 1$ quasi-Dirac neutrino model in which the lepton mixing matrix is given at tree level by the tribimaximal matrix. When radiative corrections are taken into account, new effects in neutrino oscillations, as $\nu_e \to \nu_s$, could appear. This oscillation is constrained by the solar neutrino data. In our analysis, we have found an allowed region for our two free parameters ϵ and m_1. The radiative correction, ϵ, can vary approximately from 5×10^{-9} to 10^{-6} and the calculated fourth mass eigenstate, m_4, varies in the interval 0.01–0.2 eV, at 2σ level. These results are in agreement with the ones presented in the literature in $2 + 1$ and $2 + 2$ quasi-Dirac models.

1 Introduction

The nature of the neutrino, Dirac or Majorana, is still an open question today. This notwithstanding, these are not the only options. For example, neutrinos may be Pseudo-Dirac (PD) [1–3] or Quasi-Dirac (QD) [4]. The former PD neutrinos arise when two active Majorana neutrinos are mass degenerate. In the QD neutrinos case the mass degeneration occurs with an active and a sterile neutrino.[1] This sort of neutrinos is called sterile because they do not couple to the Z and neither to the W. They only couple, in the context of the known physics, to gravity. In both cases the two Majorana mass degenerate neutrinos are equivalent to a Dirac one. The QD neutrino also may be generated if the Majorana mass term of the sterile neutrinos is smaller than the Dirac mass term. In both cases, PD and QD neutrinos, corrections

at the tree level or at the loop level will break the mass degeneracy. Generally, in models in which one of these options are implemented they are applied to all neutrinos. For instance, all the three active neutrinos are Dirac, Majorana, PD or QD particles.

An interesting QD situation happens when only one of the active neutrinos together with a sterile one are mass degenerated at tree level. In this case the three flavor states are, also at tree level, a linear combination of two massive Majorana neutrinos and the left component of a Dirac neutrino. This possibility naturally arises when S_3 symmetry is implemented in the neutrino Yukawa interactions [5–7]. In the QD scheme of Refs. [5–7] the PMNS matrix is, at tree level, the tribimaximal (TBM) [8] and the scheme is not in agreement with the recent result of a non-zero θ_{13} angle [9–11]. Thus, we can ask ourselves if in the model of Ref. [5] quantum corrections may induce an appropriate value for that mixing angle. At tree level this is possible if the S_3 symmetry is not implemented in the charged lepton Yukawa interactions and an appropriate value for θ_{13} is obtained [12]. However, quantum corrections imply, in principle, a departure from the TBM that breaks the mass degeneracy and the PMNS matrix becomes a 4×4 matrix. This implies oscillations of active neutrinos into the sterile one and, for this reason, it is mandatory to analyze how the solar neutrino data constrain the quantum corrections. The case of a QD with small Majorana masses for the sterile neutrinos was considered in Ref. [13]. However, those authors analyzed in detail only QD $2 + 1$ and $2 + 2$ schemes. It is not obvious if a QD $3 + 1$ scheme,[2] as the present one, satisfies the same constraint as shown in Ref. [13].

We know at present more about the parameters of neutrino oscillations and such knowledge is crucial for us to restructure the Standard Model. For a recent statistical analysis of all experimental neutrino data available see [14, 15].

---

[1]Usually both terms are used as synonymous in literature. However, we prefer the present notation which allows one to distinguish different mechanism in model building.

[a]e-mail: ftorres@ift.unesp.br

[b]e-mail: ana@ift.unesp.br

[c]e-mail: vicente@ift.unesp.br

---

[2]Traditionally in the literature the $3 + 1$ scheme refers to three active neutrinos and one sterile neutrino which is necessarily heavier than the others. We stress the fact that our "$3 + 1$" scheme is a quasi-Dirac one.

Moreover, since the LEP data, we know that there are only three active neutrinos [16]. Thus, an extra neutrino has to be sterile in the sense explained above. Once sterile neutrinos are added they can be of several types depending on the mass scale related with them. For a recent review of this sort of neutrinos see Refs. [17, 18]. They may be or not related to some anomalies[3] in neutrino data [19–23] or with the results of WMAP-7 [24], which indicates the existence of four relativistic species (N_{eff}).

The main objective of this paper is the following. We will apply the available solar neutrino data in a more realistic QD $3 + 1$ case, considering the possibility of electronic neutrinos (ν_e) oscillating to sterile neutrinos (ν_s). For the statistical analysis, our model has two parameters: one mass eigenstate (m_1) and the radiative correction (ϵ). This is an important difference if we compare our analysis with the one made by de Gouvêa et al. in Sect. III.A ($2 + 1$ case) [13]. Despite the differences in the model building, we have obtained an allowed region for ϵ that is similar to the corresponding values found in [13], which is $\epsilon \approx 10^{-7}$. We stress the fact that the mass splitting of the would-be Dirac neutrinos do not solve the experimental anomalies presented in [19–23], however, it is consistent with WMAP-7 results [24], since the calculated fourth mass eigenstate, m_4, varies in the interval 0.01–0.2 eV, at 2σ level.

The content of this article is the following: first, in Sect. 2 we review the basic features of our quasi-Dirac model, showing its basic structure and possible interactions with the correspondent radiative corrections to the neutrino mass matrix. In Sect. 3 we briefly describe all the solar neutrino experiments and their respective results. Also we include the method of statistical analysis used. In Sect. 4 we show in what condition the model is consistent with solar data, showing the allowed regions in the parameter space (m_1, ϵ) for our quasi-Dirac model and discussing the results. Finally, some concluding remarks are presented in Sect. 5.

2 The quasi-Dirac scheme

Recently it was shown that it is possible that all neutrino flavors are part Dirac and part Majorana [5, 6]. The latter occurs because two of the four Majorana neutrinos are mass degenerate and have opposite parity, so they are equivalent to one Dirac neutrino. As we said before, when these two neutrinos form a Dirac state and they are active, we call them pseudo-Dirac neutrinos. When there is one active and one sterile, they are called quasi-Dirac neutrinos. The other two have distinct Majorana masses. In our particular model, we

point out that there are initially three right-handed neutrinos. Two of them are integrated and we obtain a model QD "3 + 1"—three active neutrinos and one sterile.

In this section we are briefly going to describe the construction of our model (Sect. 2.1). In Sect. 2.2, we show the main interactions that are going to be used to obtain the radiative corrections for the neutrino masses. These radiative corrections are very important to our analysis: we study their effects on the break of the degeneracy between the two Majorana neutrinos that form a Dirac neutrino at tree level. For more details of the model building that we have used here, see [5, 12].

2.1 The model

The model we are going to present here is based on a gauged $B - L$ symmetry with a quasi-Dirac neutrino in which the right-handed neutrinos carry exotic local $B - L$ charges [5, 12].

When the S_3 symmetry is added to the model, the left-handed leptons belong to the reducible triplet representation ($3 = (L_e, L_\mu, L_\tau)$) since all of them have the same $B - L$ charge.

However, unlike the usual case when the three right-handed neutrinos have $L = 1$, in this model they have different $B - L$ charge, so they can transform under S_3 only as a singlet $1 = n_{\mu R}$ with $B - L = -4$, and a doublet, $2 = (n_{eR}, n_{\tau R})$, with $B - L = 5$. In the neutrino Yukawa sector, the S_3 triplet, (L_e, L_μ, L_τ), can be decomposed into irreducible representations as $3 = 1 + 2$, then we can write the singlet and doublet as follows:

$$L_2 = \frac{1}{\sqrt{3}}(L_e + L_\mu + L_\tau) \sim 1,$$

$$(L_1, L_3) = \left(\frac{1}{\sqrt{6}}(2L_e - L_\mu - L_\tau), \frac{1}{\sqrt{2}}(L_\mu - L_\tau) \right) \sim 2. \tag{1}$$

The scalar sector has two scalar doublets of $SU(2)$ with weak hypercharge $Y = -1$ that are denoted by $\Phi_{1,2} = (\varphi_{1,2}^0 \, \varphi_{1,2}^-)^T$. They are singlets of S_3 and we will denote $\langle \varphi_1^0 (\varphi_2^0) \rangle = v_1(v_2)/\sqrt{2}$. If $n_{\mu R}$ is considered light, but n_{eR} and $n_{\tau R}$ heavy (with masses m_{n_e} and m_{n_τ}, respectively), we can integrate out the heavy degrees of freedom. After that, the effective lepton Yukawa interactions are given by a dimension five effective Lagrangian plus a Dirac mass term, as follows:

$$-\mathcal{L}_\nu^{eff} = h_1 \bar{L}_2 \Phi_1 n_{\mu R} + \frac{h_2^2}{m_{n_e}} \left[\overline{(L_1^c)}_R \Phi_2^* \right] [L_{1L} \Phi_2^*]$$

$$+ \frac{h_3^2}{m_{n_\tau}} \left[\overline{(L_3^c)}_R \Phi_2^* \right] [L_{3L} \Phi_2^*] + H.c., \tag{2}$$

where the mixing angles in the ($n_{eR}, n_{\tau R}$) sector have been absorbed in the dimensionless couplings, h_2 and h_3.

---

[3]When we refer to neutrino anomalies we are talking about the need of more families to explain the results of, for example, LSND and Mini-BooNE experiments and others that require $\Delta m^2 > 0.1$ eV^2.

From the Yukawa interactions in (2), we obtain the mass matrix in an appropriate basis [5], $(\nu_e\ \nu_\mu\ \nu_\tau\ n^c_\mu)_L$. At tree level the mass matrix is diagonalized by the following 4×4 matrix:

$$U_0 = \begin{pmatrix} U_{\text{TBM}} & 0_{3\times 1} \\ 0_{1\times 3} & 1 \end{pmatrix}, \tag{3}$$

where U_{TBM} is the tribimaximal matrix and 0 denote the matrix row or column with entries equal to zero.

Since the model has more interactions than those in the Standard Model, the neutrino mass matrix, when radiative corrections are taken into account, is not necessarily diagonalized by U_0, written in Eq. (3), but for $U_0 \to U$, where U is now another 4×4 matrix which, in principle, is not of the TBM type. In fact the main objective of this paper is verify if the appropriate value for θ_{13} could arise only from perturbation of the TBM mixing matrix through radiative corrections and keeping agreement with solar neutrino data. This can be obtained in two different manners: (1) if (V_{PMNS}), which is now a 4×4 matrix, is such that $(V_{\text{PMNS}})_{13}$ has the correct value and $(V_{\text{PMNS}})_{14} \sim 0$; or (2) both $(V_{\text{PMNS}})_{13}$ and $(V_{\text{PMNS}})_{14}$ are different from zero but there is a non-negligible active neutrino into sterile neutrino oscillation. This would imply the disappearance of $\bar{\nu}_e$ in agreement with experimental data from Daya Bay, RENO and Double-Chooz.

2.2 Quantum corrections

When radiative corrections are taken into account—see Fig. 1—the neutrino mass matrix can be written as

$$M^\nu = M^{0\nu} + \Delta M^\nu, \tag{4}$$

where $M^{0\nu}$ is the mass matrix at tree level [12] and ΔM^ν arises from 1-loop corrections. In order to calculate the mass
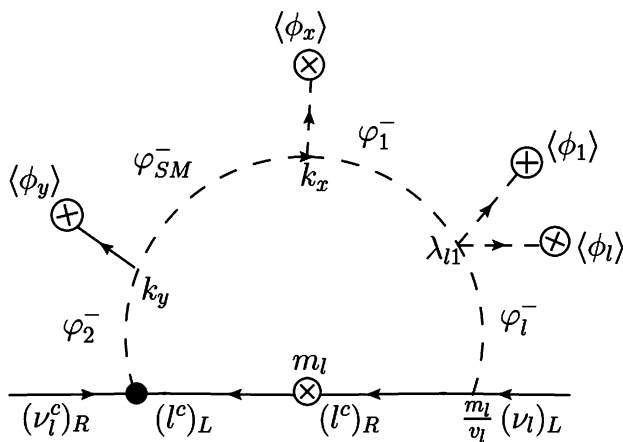

Fig. 1 A 1-loop contribution for the Majorana mass matrix in the flavor basis induced by charged scalars. The ● in the *left* vertex denotes interactions in Eq. (5)

corrections, ΔM^ν, we have to consider all the Yukawa interactions in the lepton and scalar sectors. From Eq. (2) the scalar-charged lepton interactions are

$$-\mathcal{L}^{l\nu\phi}_{CC} = \frac{m_D}{\sqrt{3}v_1}(\bar{e}_L + \bar{\mu}_L + \bar{\tau}_L)(\nu^c_D)_R\varphi^+_1$$
$$- \Bigg[\frac{1}{\sqrt{6}}\frac{m_1}{v^2_2}[2\overline{(e^c)}_R + \overline{(\mu^c)}_R + \overline{(\tau^c)}_R]\nu_{1L}$$
$$- \frac{1}{\sqrt{2}}\frac{m_3}{v^2_2}[\overline{(\mu^c)}_R - \overline{(\tau^c)}_R]\nu_{3L}\Bigg]$$
$$\times \frac{1}{\sqrt{2}}(v^*_2 + \text{Re}\varphi^{0*}_2 + i\text{Im}\varphi^{0*}_2)\varphi^+_2 + H.c. \tag{5}$$

and we have used $\nu^M_{(1,3)L} = \nu_{(1,3)L}$, $\nu^M_{2L} = \nu_{2L}$, $\sqrt{2}(\nu^c_D)_R = n_{\mu R}$. The notation is as follows: m_1 and m_3 are the Majorana masses, while m_D is the common mass to the degenerated Majorana neutrinos, all of them at the tree level.

The Yukawa interactions from which the charged leptons get mass are mainly the diagonal ones,

$$\mathcal{L}^l_{\text{yukawa}} \approx G\sum_l (\bar{\nu}_l\ \bar{l})^\dagger_L \Phi_l l_R + H.c. \tag{6}$$

where $\Phi_l = (\varphi^+_l\ \varphi^0_l)^T$, and $l = e, \mu, \tau$, where G is a dimensionless constant. The charged lepton mass matrix is almost diagonal [5], hence $m_l \approx Gv_l$, and the neutrino interactions with charged leptons are given by $(m_l/v_l)\bar{\nu}_{lL}l_R\varphi^+_l$. We stress the fact that it is the neutrino flavor basis that is important here. On the other hand, the scalar potential includes the following interactions:

$$V(\Phi_1, \Phi_2, \ldots)$$
$$\propto \lambda_{1l}\Phi^\dagger_l\Phi_1\Phi^\dagger_1\Phi_l + \lambda_{2l}\Phi^\dagger_l\Phi_2\Phi^\dagger_2\Phi_l$$
$$+ k_x\Phi^T_1\varepsilon\Phi_{SM}\phi_x + k_y\Phi^T_2\varepsilon\Phi_{SM}\phi_y + H.c., \tag{7}$$

where $l = e, \mu, \tau$. In Eq. (7), Φ_{SM} denotes a scalar doublet with $Y = +1$ and without $B - L$ charge, and ϕ_x, ϕ_y are scalars carrying also $B - L$ charges [5]. k_x and k_y are coupling constants with mass dimension and ε is the antisymmetrical tensor.

With the interactions in Eqs. (5), (6), and (7), we obtain diagrams like the one in Fig. 1. As we mentioned before, these sort of diagrams provide corrections to the Majorana masses for the active neutrinos, i.e., $\overline{(\nu_{aL})^c}\nu_{bL}$. Also corrections to the Dirac mass terms $\bar{\nu}_{aL}n_{\mu R}$ arise from diagrams similar to the one shown in Fig. 1. The 1-loop corrections to the neutrino mass matrix (M^ν) in $\chi'_i = N'_{iL} + (N'_{iL})^c$ basis where $N'_{iL} = (\nu_e\ \nu_\mu\ \nu_\tau\ n^c_\mu)^T_L$ are written in the following:

$$M^\nu = m_1 \begin{pmatrix} \frac{2}{3}(1-\epsilon_e) & -\frac{1}{3}(1-2\epsilon_e) & -\frac{1}{3}(1-2\epsilon_e) & \frac{m_D}{\sqrt{3}m_1}(1+\epsilon_e') \\ -\frac{1}{3}(1-2\epsilon_\mu) & (\frac{1}{6}+\frac{m_3}{2m_1})(1+2\epsilon_\mu) & (\frac{1}{6}-\frac{m_3}{2m_1})(1+\epsilon_\mu) & \frac{m_D}{\sqrt{3}m_1}(1+\epsilon_\mu') \\ -\frac{1}{3}(1-\epsilon_\tau) & (\frac{1}{6}-\frac{m_3}{2m_1})(1+\epsilon_\tau) & (\frac{1}{6}+\frac{m_3}{2m_1})(1+\epsilon_\tau) & \frac{m_D}{\sqrt{3}m_1}(1+\epsilon_\tau') \\ \frac{m_D}{\sqrt{3}m_1}(1+\epsilon_e') & \frac{m_D}{\sqrt{3}m_1}(1+\epsilon_\mu') & \frac{m_D}{\sqrt{3}m_1}(1+\epsilon_\tau') & 0 \end{pmatrix}. \tag{8}$$

From Eq. (6), $G = m_e/v_e = m_\mu/v_\mu = m_\tau/v_\tau$, we can express the radiative corrections as

$$\epsilon_l = \frac{1}{8\sqrt{2}\pi^2}\frac{v_1}{v_2}\lambda_{1l}m_l^2 AB_l\big[m_l^2\big[1-\ln(m_l^2/m_{\varphi_2^+}^2)\big]$$
$$- m_{\varphi_2^+}^2 + C_l \ln(C_l/m_{\varphi_2^+}^2)\big],$$
$$\epsilon_l' = \frac{1}{8\pi^2}\frac{v_2}{v_1}\lambda_{2l}m_l^2 AB_l\big[m_l^2\big[1-\ln(m_l^2/m_{\varphi_2^+}^2)\big]$$
$$- m_{\varphi_2^+}^2 + C_l \ln(C_l/m_{\varphi_2^+}^2)\big]. \tag{9}$$

When all ϵ's and ϵ'''s in Eq. (8) are equal to zero, the mass matrix is the same as the one represented at tree level.

In Eq. (9), A, B_l, and C_l are given by

$$A = \frac{\sqrt{3}\,k_x k_y \langle\phi_x\rangle\langle\phi_y\rangle}{m_{\varphi_2^+}^6},$$

$$B_l = \frac{m_{\varphi_2^+}^6}{2(m_l^2-m_{\varphi_1^+}^2)(m_l^2-m_{\varphi_2^+}^2)(m_l^2-m_{\varphi_l^+}^2)(m_l^2-m_{\varphi_{SM}^0}^2)}, \tag{10}$$

$$C_l = m_{\varphi_l^+}^2 + m_{\varphi_2^+}^2 + m_{\varphi_1^+}^2 + m_{\varphi_3^+}^2 - 5m_l^2.$$

In Eq. (10), $m_{\varphi_i^+}$ are the charged scalar masses and m_l are the charged lepton masses.

The general form of the mass matrix in Eq. (8) is very complicate to treat, so we will do some approximations in order to simplify our analysis. As we can see in Eqs. (10), we have six dimensionless free parameters: λ_{1l} and λ_{2l}, where $l = e, \mu, \tau$. Instead of choose the value of each one independently, we use two conditions denoted as CASE A and CASE B, detailed below, and then we have their respective values defined. However, we stress that this numerical choice is not relevant and crucial for our analysis.

1. *CASE A*: $\lambda_{1e}m_e^2 = \lambda_{1\mu}m_\mu^2 = \lambda_{1\tau}m_\tau^2 \equiv M_1^2$ and $\lambda_{2e}m_e^2 = \lambda_{2\mu}m_\mu^2 = \lambda_{2\tau}m_\tau^2 \equiv M_2^2$. We will also assume that $M_1 \approx M_2 \sim 0.001$ GeV. Note that for this case the value for $\lambda_{1e} \sim \lambda_{2e} < 4$, and the value for the others is even lower.

In this case we have $\epsilon_e = \epsilon_\mu = \epsilon_\tau = \epsilon$ and $\epsilon_e' = \epsilon_\mu' = \epsilon_\tau' \equiv \epsilon'$ and

$$\epsilon \approx \frac{\sqrt{3}}{16\pi^2}\frac{v_1}{v_2}\frac{k_x k_y \langle\phi_x\rangle\langle\phi_y\rangle M_1^2}{m_{\varphi_{SM}}^2 M^4},$$
$$\epsilon' \approx \frac{v_2^2}{\sqrt{2}v_1^2}\epsilon. \tag{11}$$

M is a typical mass in the charged scalar sector and $m_{\varphi_{SM}^0}^2$ is the mass square of the Higgs of the SM. We will use all the scalar masses equal to 125 GeV. In this condition we have

$$\epsilon = \frac{5\times10^{-21}}{\text{GeV}^4}\,k_x k_y \langle\phi_x\rangle\langle\phi_y\rangle,$$
$$\epsilon' = \frac{7\times10^{-21}}{\text{GeV}^4}\,k_x k_y \langle\phi_x\rangle\langle\phi_y\rangle, \tag{12}$$

where $k_{x,y}$ and $\phi_{x,y}$ are in GeV units. For $\epsilon \lesssim 1$ we need $k_x k_y \langle\phi_x\rangle\langle\phi_y\rangle \sim 10^{20}\,\text{GeV}^4$ which implies four mass scale of the order of 100 TeV, or at least two masses in the scale of the grand unification. We recall that these dimensional parameters are not related to the electroweak scale. Hence, we have put our ignorance about the real values for the parameters in terms of the scalar sector that is not constrained by the electroweak scale.

2. *CASE B*: $\lambda_{1e}m_e = \lambda_{1\mu}m_\mu = \lambda_{1\tau}m_\tau \equiv M_1$ and $\lambda_{2e}m_e = \lambda_{2\mu}m_\mu = \lambda_{2\tau}m_\tau \equiv M_2$. With the same assumption of the CASE A we have

$$\epsilon_l = \frac{5\times10^{-20}}{\text{GeV}^5}\,k_x k_y \langle\phi_x\rangle\langle\phi_y\rangle m_l,$$
$$\epsilon_l' = \frac{7\times10^{-20}}{\text{GeV}^5}\,k_x k_y \langle\phi_x\rangle\langle\phi_y\rangle m_l, \tag{13}$$

where $k_{x,y}$ and $\phi_{x,y}$ are in GeV units. In this case we have a certain hierarchy in the radiative corrections ($\epsilon_e \ll \epsilon_\mu \ll \epsilon_\tau$). The radiative corrections ϵ_τ and ϵ_τ' can be $\lesssim 1$ and

$$\epsilon_e = \frac{m_e}{m_\tau}\epsilon_\tau, \qquad \epsilon_\mu = \frac{m_\mu}{m_\tau}\epsilon_\tau,$$
$$\epsilon_e' = \frac{m_e}{m_\tau}\epsilon_\tau', \qquad \epsilon_\mu' = \frac{m_\mu}{m_\tau}\epsilon_\tau', \tag{14}$$

note that for this case the value for $\lambda_{1e} \sim \lambda_{2e} < 2$, and the value for the others is even lower.

We are going to use both of these approximations in the following analysis. Therefore, we have two main free parameters which were written in Eq. (8): the mass m_1 (in eV units) and the radiative corrections (dimensionless) parameter, ϵ for the CASE A; and $\epsilon_\tau = \epsilon$ and $\epsilon'_\tau = \epsilon'$ for the CASE B. For this case, the other ϵ's and ϵ''s are calculated by Eq. (14). We notice that $\epsilon_\tau \approx \epsilon'_\tau$, then we are going to express our results, for the CASE B, using $\epsilon_\tau = \epsilon$.

This notwithstanding, it is necessary to analyze how the solar neutrino data constraint the values of ϵ's since there are active to sterile neutrino oscillation. This is the issue of the next section.

3 Solar neutrinos constraints

The detection of neutrinos traveling from the sun has given us a tremendous evidence of neutrino oscillation. We might say that it was the first time that physicists were doing astronomy with neutrinos and several aspects of the solar behavior have being observed and understood since then. From Homestake to SNO, nowadays we have a considerable amount of significant data, which also gives us the opportunity to use this fact to constrain and test the validity of models. This is exactly what we are going to do: constraining the parameters of the quasi-Dirac model presented in Sect. 2 and checking its validity in confrontation with the solar neutrino data. This data is taken from the following experiments: Homestake [25], Gallex/GNO [26], Sage [27], Kamiokande [28], Super-Kamiokande [29], SNO [30] and Borexino [31]. In Sect. 3.1 we are going to present a small review about these experiments and their main numerical results. In Sect. 3.2 we present how to treat the oscillation physics of solar neutrinos and the main points of our statistical analysis. For recent reviews on solar neutrinos see [32–34].

3.1 Experimental data

For the statistical analysis, Sect. 3.2, we are going to consider the entire set of the solar neutrino data presented in Table 1. This table presents each solar neutrino experiment and the measured flux (ϕ_{exp}). Depending on the experiment, the flux is measured by charged, neutral current reaction and elastic scattering.

Elastic scattering experiments, $\nu_a + e^- \rightarrow \nu_a + e^-$ ($a = e, \mu, \tau$), include Kamiokande [28], Super-Kamiokande [29], Borexino [31, 35]. Kamiokande and Super-Kamiokande detected ^8B neutrinos with threshold of 7.5 MeV and 5 MeV, respectively. Borexino, on the other hand, detects neutrinos from the ^7Be line with an energy of 0.86 MeV. Recently, Borexino has also measured for the first time the flux of low energy *pep* neutrinos: $\phi_{pep} = (1.6 \pm 0.3) \times 10^8$ cm^{-2} s^{-1} [36]. However, we do not use this value in our analysis.

SNO experiment [30] detects electronic neutrinos in a charged current reaction, $\nu_e + d \rightarrow p + p + e^-$ (threshold of 5 MeV). Also, there is the detection of other neutrino flavors by neutral current reaction, $\nu_a + d \rightarrow n + p + \nu_a$ (threshold of 2.225 MeV), and elastic cross section. SNO had three stages and obtained different fluxes [37–39] shown in Table 1.

We used also the Homestake experiment [25], $\nu_e + ^{37}Cl \rightarrow ^{37}Ar + e^-$ (threshold of 0.814 MeV), and the ^{71}Ga experiments: GALLEX/GNO [26] and SAGE [27] (threshold of 0.233 MeV). In Table 1, we referred to all gallium experimental results [40]. We notice that they are sensitive to almost the entire neutrino solar spectrum.

Table 1 Resume of solar neutrino data. Also including the experimental uncertainties

Experiment	Experimental data
Homestake [25]	$2.56 \pm 0.16 \pm 0.16$ SNU[a]
Gallex/GNO and Sage [40]	68.1 ± 3.75 SNU
Kamiokande [28]	$\phi_{Kam} = (2.80 \pm 0.19 \pm 0.33) \times 10^6$ cm^{-2} s^{-1}
SK [29]	$\phi_{SK} = (2.35 \pm 0.02 \pm 0.08) \times 10^6$ cm^{-2} s^{-1}
SNO—D_2O [37]	$\phi_{CC} = (1.76^{+0.06}_{-0.05}(\text{stat.})^{+0.09}_{-0.09}(\text{syst.})) \times 10^6$ cm^{-2} s^{-1}
	$\phi_{ES} = (2.39^{+0.24}_{-0.23}(\text{stat.})^{+0.12}_{-0.12}(\text{syst.})) \times 10^6$ cm^{-2} s^{-1}
	$\phi_{NC} = (5.09^{+0.44}_{-0.43}(\text{stat.})^{+0.46}_{-0.43}(\text{syst.})) \times 10^6$ cm^{-2} s^{-1}
SNO—NaCl [38]	$\phi_{CC} = (1.59^{+0.08}_{-0.07}(\text{stat.})^{+0.06}_{-0.08}(\text{syst.})) \times 10^6$ cm^{-2} s^{-1}
	$\phi_{ES} = (2.21^{+0.31}_{-0.26}(\text{stat.}) \pm 0.10(\text{syst.})) \times 10^6$ cm^{-2} s^{-1}
	$\phi_{NC} = (5.21 \pm 0.27(\text{stat.}) \pm 0.38(\text{syst.})) \times 10^6$ cm^{-2} s^{-1}
SNO—^3He [39]	$\phi_{CC} = (1.67^{+0.05}_{-0.04}(\text{stat.})^{+0.07}_{-0.08}(\text{syst.})) \times 10^6$ cm^{-2} s^{-1}
	$\phi_{ES} = (1.77^{+0.24}_{-0.21}(\text{stat.})^{+0.09}_{-0.10}(\text{syst.})) \times 10^6$ cm^{-2} s^{-1}
	$\phi_{NC} = (5.54^{+0.33}_{-0.31}(\text{stat.})^{+0.36}_{-0.34}(\text{syst.})) \times 10^6$ cm^{-2} s^{-1}
Borexino [31]	$\phi = (4.84 \pm 0.24) \times 10^9$ cm^{-2} s^{-1}

[a] 1 SNU $= 10^{-36}$ captures/atom/sec

3.2 Analysis

Neutrinos are produced for several thermal nuclear reactions in the center of the sun [41, 42] and we present them in Table 2 extracted from [43]. The energy of these neutrinos are of a few MeV. To be accurate, we must treat the center of the sun as a region where the chemical composition modifies itself with the radius. So each reaction produces a different flux of neutrinos and this changes, as we pointed out, with the position from the center of the sun. Neutrino sources are pp, hep, pep, ^{13}N, ^{15}O, ^{17}F, ^{8}B, and ^{7}Be. Details of the distribution of the neutrino production as a function of the radius for each of the solar neutrino sources can be found in [41, 42] and we used this profile in our work to average the oscillation probabilities, since detectors only "see" these averages.

After electronic neutrinos (ν_e) are produced by several reactions and in different points of the core of the sun, they will propagate inside the sun, which has a radius $R_{\text{sun}} \approx 6.9 \times 10^{10}$ cm. This propagation is described by the effective Hamiltonian of the system in the flavor state base:

$$H_{\text{eff}}(r) = \frac{M^\nu (M^\nu)^\dagger}{2E} + V(r). \quad (15)$$

We emphasize that $M^\nu = M^\nu(\epsilon, m_1)$ is taken from Eq. (8), $V(r)$ is the potential of the neutrino interaction with the solar environment, E is the ν_e energy and r is the distance from the center of the sun. The potential, $V(r)$, can be written as the sum of the charged current and neutral current interaction ($V(r) = V_{cc}(r) + V_{nc}(r)$), which are dependent on the electronic density ($n_e(r)$) and neutron density ($n_n(r)$) of the environment. Both of these quantities change with the distance from the solar core and can be written as

$$V(r) = V_{cc}(r) + V_{nc}(r) = \sqrt{2}G_F\left(n_e(r) - \frac{1}{2}n_n(r)\right). \quad (16)$$

The profile of $n_e(r)$ and $n_n(r)$ used in our analysis has been extracted from [41, 42] and G_F is the Fermi coupling constant.

The survival probability (P_{ee}), for each energy and in each point of neutrino production, is calculated from the amplitude A_{ee}, which can be written as

$$A_{ee} = (1\ 0\ 0\ 0)\, U_{\text{vac}} \times \text{diag}\big(\exp\left(-i\Phi'_1\right), \exp\left(-i\Phi'_2\right),$$
$$\exp\left(-i\Phi'_3\right), \exp\left(-i\Phi'_4\right)\big)$$
$$\times \begin{pmatrix} 1 & 0 & 0 & 0 \\ 0 & \sqrt{1-P_c} & 0 & -\sqrt{P_c} \\ 0 & 0 & 1 & 0 \\ 0 & \sqrt{P_c} & 0 & \sqrt{1-P_c} \end{pmatrix}$$
$$\times \text{diag}\big(\exp\left(-i\Phi_1\right), \exp\left(-i\Phi_2\right), \exp\left(-i\Phi_3\right),$$
$$\exp\left(-i\Phi_4\right)\big) \times U^\dagger_{\text{mat}}\begin{pmatrix} 1 \\ 0 \\ 0 \\ 0 \end{pmatrix}. \quad (17)$$

So the survival probability is written as $P_{ee} = |A_{ee}|^2$. In Eq. (17), $U_{\text{mat}} \equiv U_{\text{mat}}(\epsilon, m_1, E)$ is the matter mixing matrix which diagonalizes the effective Hamiltonian represented by Eq. (15). The crossing probability, which will be discussed later, is represented by P_c. The matrix $U_{\text{vac}} \equiv U_{\text{vac}}(\epsilon, m_1)$ is the vacuum mixing matrix which diagonalizes Eq. (15) when $V(r)$ is equal to zero (vacuum regime). If we take $\epsilon = 0$, no radiative corrections, for any m_1 value, U_{vac} is going to be the tribimaximal mixing matrix. As the elements of U_{vac}, the elements of U_{mat} are modified by the choice of the parameters ϵ and m_1. When the electronic neutrinos travel to less dense regions of the sun, $U_{\text{mat}} \to U_{\text{vac}}$. The phases Φ_i represent the evolution of the mass eigenstates in matter. We express this as $\Phi_i = \int_{r_0}^{R_{\text{sun}}} \mu_i^2(x)/(2E)\,dx$, where $\mu_i^2(x)$ ($i = 1, 2, 3, 4$) is the mass eigenvalue of Eq. (15) and r_0 is the neutrino point of production. The phase Φ'_i has a similar meaning as Φ_i, but for the vacuum propagation. We discuss it later in this section.

In Fig. 2, we show the evolution of the mass eigenstates in the sun for a neutrino with energy $E = 5$ MeV, $m_1 = 0.001$ eV, $\epsilon = 1.0 \times 10^{-3}$. The solid black curve represents the mass eigenstate μ_1; dotted blue, dashed green and

Table 2 Sources of solar neutrinos: first column represents the name of the source which produces the electronic neutrino inside the sun; the second column shows the resume reaction; the third and fourth columns represent, respectively, the average neutrino energy and the maximum neutrino energy

Source	Reaction	Average ν energy (MeV)	Maximum ν energy (MeV)
pp	$p + p \to d + e^+ + \nu_e$	0.27	0.42
pep	$p + e^- + p \to d + \nu_e$	1.44	1.44
hep	$^3\text{He} + p \to {}^4\text{He} + e^+ + \nu_e$	9.63	18.78
^{7}Be	$e^- + {}^7\text{Be} \to {}^7\text{Li} + \nu_e$	0.86	0.86
^{8}B	$^8\text{B} \to {}^8\text{Be}^* + e^+ + \nu_e$	6.74	15.00
^{13}N	$^{13}\text{N} \to {}^{13}\text{C} + e^+ + \nu_e$	0.71	1.19
^{15}O	$^{15}\text{O} \to {}^{15}\text{N} + e^+ + \nu_e$	0.99	1.73
^{17}F	$^{17}\text{F} \to {}^{17}\text{O} + e^+ + \nu_e$	0.99	1.74

Fig. 2 Evolution of the mass eigenstates inside the Sun. For this plot we use $\epsilon = 1.0 \times 10^{-3}$, $E = 5$ MeV, and $m_1 = 0.001$ eV. *Black solid curve is for* μ_1; *blue dotted one for* μ_2; *green dashed curve for* μ_4 *and red dot-dashed is for* μ_3
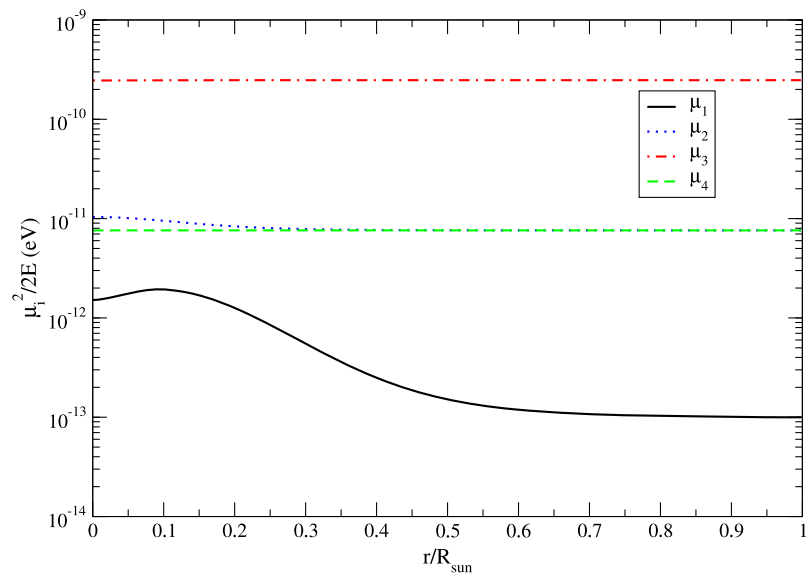
dot-dashed red ones represent μ_2, μ_4 and μ_3, respectively.[4] We notice that ν_2 and ν_4 are practically degenerate, which is the most important characteristic of quasi-Dirac models. It is also possible to notice that matter can break this degeneracy for very small radius as we can notice in Fig. 2. However, for very small ϵ, we see that ν_2 and ν_4 are practically degenerate, generating a Δm^2_{42} that can be sensible to oscillations: $\Delta m^2_{42} L/(2E) \sim 1$, where L is the Sun–Earth distance, which is about 150 million kilometers.

For instance, in the limit of $\epsilon \to 0$, we recover the original and standard 3×3 situation without the sterile neutrino presence, where the terms U_{e1} and U_{e2} solve properly the solar neutrino problem: the deficit of ν_e arriving the Earth. For $\epsilon \neq 0$ and small, it is important to notice that ν_2 and ν_4 will be a coherent mixture—$(\nu_2 + i\nu_4)/\sqrt{2}$—and this is an eigenstate of the Hamiltonian in vacuum.

We know that the mass eigenstates can feel MSW resonances during the propagation [44, 45]. When neutrinos go through the MSW resonance, the conversion probability is maximal. We remember that conversion probabilities are obtained using the expression written in Eq. (17), but changing the position of the number "1" of the line vector (1 0 0 0). For example, $P_{e\mu}$ is obtained using the line vector (0 1 0 0). In principle, we can have resonances among all the mass eigenstates, however, ν_3 is the heaviest and it will not suffer resonance—its propagation is adiabatic. Also, we can say that the scale Δm^2_{3i}, with $i = 1, 2, 4$, can be averaged out. In other words, this mass squared difference scale is not important for the solar neutrino oscillation phenomenon. The moment of the resonance is represented by the matrix that

contains P_c in Eq. (17). This P_c is the crossing probability, which represents the probability of a mass eigenstate ν_i be converted to another mass eigenstate ν_j. In the standard neutrino oscillation case, if the propagation is adiabatic, we must have $P_c = 0$. In other words, there is no conversion between two mass eigenstates. In the instantaneous mass basis (ν_i^m, for $i = 1, 2, 3, 4$), where ν^m is the neutrino state in matter, the evolution equation is expressed as:

$$i\frac{d\nu^m}{dx} = \left[\frac{1}{2E}\text{diag}\big(\mu_1^2(x), \mu_2^2(x), \mu_3^2(x), \mu_4^2(x)\big) - iU_m^\dagger(x)\frac{dU_m(x)}{dx} \right],$$

(18)

where $\mu_i^2(x)$ is the effective mass eigenstate calculated from the eigenvalues of Eq. (15). If the last term of Eq. (18) is significant compared with the first one, non-adiabatic transition can happen. The adiabaticity parameter, represented by the letter γ, is evaluated at the resonance point, for simplicity, and is defined as

$$\gamma_{ij} = \left| \frac{\frac{(\mu_j^2(x) - \mu_i^2(x))}{2E}}{[U_m^\dagger(x)\frac{dU_m(x)}{dx}]_{ij}} \right|.$$

(19)

When $\gamma_{ij} \ll 1$ ($\gamma_{ij} \gg 1$), the propagation is non-adiabatic (adiabatic). Considering ν_1 and ν_2 (or ν_4, since they are practically degenerate), for any values of ϵ and m_1, and evaluating Eq. (19), we conclude that MSW resonance and all the propagation is adiabatic. Actually, for $\epsilon \to 0$, mixing angles and mass squared differences extracted from our model are very close to the experimental ones [16], so we know from experiments that the propagation is adiabatic. As an example, we can see in Fig. 3, evaluated for $E = 5$ MeV, $\epsilon = 0.8$, and $m_1 = 0.001$ eV, that γ_{12} (solid black curve) is

---

[4]The use of the Greek letter μ_i is generally used to represent the mass eigenstates in matter; m_i, on the other hand, is usually used to represent the neutrino mass eigenstates in vacuum.

Fig. 3 Parameter of adiabaticity for the $\nu_1 \to \nu_2$ (*solid black curve*) and $\nu_2 \to \nu_4$ (*red dashed curve*) transitions, using $\epsilon = 0.8$, $E = 5$ MeV, and $m_1 = 0.001$ eV
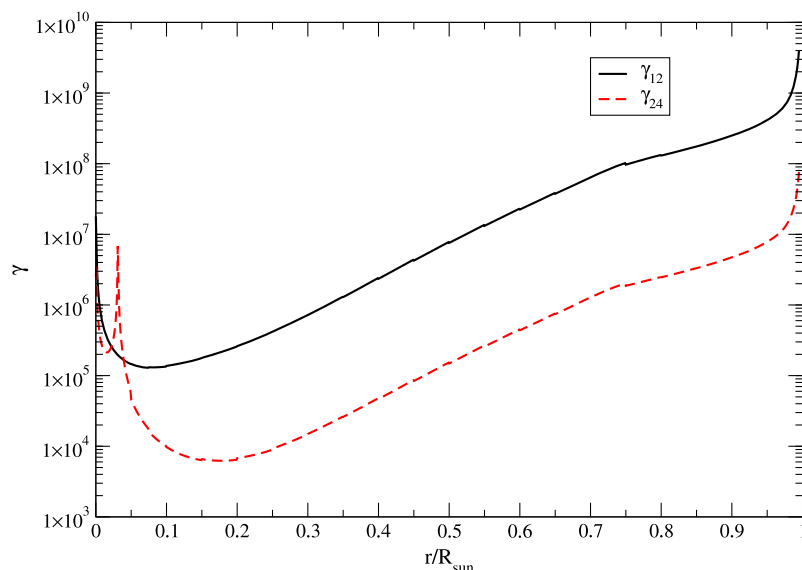
very large and much greater than 1. Then we can say that Fig. 3 has showed, even for large ϵ, that the value of γ_{12} is kept large and then the propagation remains adiabatic. Even for larger values of m_1 we obtain the same pattern and magnitude of γ_{12}. We also can say that Fig. 3 represents the behavior and magnitude for γ_{14}. However, since we have a (quasi-)degenerate state between ν_2 and ν_4, $m_2 \approx m_4$, we cannot say that this transition is always adiabatic. So, $\nu_2 \leftrightarrow \nu_4$ is very dependent on the values of ϵ and m_1. In Fig. 3, γ_{24} (dashed red curve) is also very high for the ϵ, m_1 and E values that we chose. This transition, for this particular choice, is also adiabatic. The modification in the pattern of the curve is related with the modification in the values of the denominator in Eq. (19), but this does not modify the adiabatic propagation. When ϵ becomes smaller, the adiabaticity γ_{24} tends to break. We need to compute Eq. (19) and calculate the crossing probability, P_c, for this kind of transition.

The crossing probability can be written as [46]

$$P_c = \frac{e^{-\frac{\pi}{2}\gamma|U_{(\text{vac})24}|^2} - e^{-\frac{\pi}{2}\gamma}}{1 - e^{-\frac{\pi}{2}\gamma}}, \tag{20}$$

where $U_{(\text{vac})24}$ is the 24 element of the mixing matrix in vacuum and $\gamma = \gamma_{24}$. If γ is large, we have an adiabatic propagation of ν_2 and ν_4, and they will get out independently of the sun, as distinct mass eigenstates. Then, in this situation, $P_c = 0$. On the other hand, with a very small γ, which generally happens for very small ϵ, we have a non-adiabatic propagation of ν_2 and ν_4, and they will get out of the sun, as mentioned before, as a coherent mixture. Then in this situation, $P_c = 0.5$.

After the propagation inside the sun, neutrinos will travel in vacuum, with a phase Φ'_i, $i = 1, 2, 3, 4$—see Eq. (17)—where $\Phi'_i = \int m_i^2/(2E)\,dx$ and m_i is the neutrino mass

eigenstate in vacuum. The integration is taken along all the path from sun to Earth. Only Δm_{24}^2 is considered, for certain values of ϵ and m_1, and cannot be averaged out. Other mass squared differences are averaged out since $\Delta m^2 L/(2E) \gg 1$. It is important to stress out that we are ignoring Earth matter effects. An extended analysis involving four neutrino families with a great variety of Δm_{14}^2 and mixing angles was done in [47].

The general expression of the expected event rate in the presence of oscillations in experiment j in the four neutrino framework is given by R_j^{th}:

$$R_j^{\text{th}} = \sum_{k=1,8} \phi_k \int dE\, \lambda_k(E) \times \big[\sigma_{e,i}(E)\langle P_{ee}\rangle$$
$$+ \sigma_{x,i}(E)\big(1 - \langle P_{ee}\rangle - \langle P_{ea}\rangle\big)\big], \tag{21}$$

where E is the neutrino energy, ϕ_k and λ_k are, respectively, the total neutrino flux and the neutrino energy spectrum normalized to one from the solar nuclear reaction k with normalization given by the model BS05(OP) in [41, 42]—see Table 2. In Eq. (21), $\sigma_{e,i}$ ($\sigma_{x,i}$) is the ν_e (ν_x, $x = \mu, \tau$) interaction cross section in the Standard Model with the target corresponding to experiment j, $\langle P_{ee}\rangle$ is the average survival probability in the production point, $\langle P_{ea}\rangle$ and $\langle P_{es}\rangle$ are, respectively, the average conversion probability in the production point of $\nu_e \to \nu_a$ ($a = \mu, \tau$) and $\nu_e \to \nu_s$.

The χ^2 test is calculated by

$$\chi^2 = \sum_j \frac{(R_{\text{th}}^j - R_{\text{exp}}^j)^2}{\sigma_j^2}, \tag{22}$$

where R_{exp}^j is the experimental rate for j-experiment—see Table 1. Generally, the rate is defined as $R = \phi/\phi_{\text{SSM}}$, where

ϕ_{SSM} is the total flux of the solar standard model extracted from the model BS05(OP) [41, 42]: R_{th} corresponds to a ϕ_{th} that represents the oscillated flux, which is related to the parameters of our model and evaluated using Eq. (21); R_{exp} is based on the flux ϕ_{exp}, which is the experimental value extracted from Table 1. The χ^2 is calculated for each set of ϵ and m_1. Note in Eq. (22) that σ_j^2 is the error, which takes into account the experimental error of a particular experiment and errors associated with the flux expectations in BS05(OP).

4 Results

From Eq. (17), we plot the probabilities for two sets of parameters (m_1, ϵ) for the CASE A. In Fig. 4, we used as input $\epsilon = 5.0 \times 10^{-7}$ and $m_1 = 0.003$ eV. The masses m_2 and m_3, which appear in Eq. (8), are calculated. To maintain hierarchy, for which we choose the normal one for simplicity, the masses m_2 and m_3 will be written as follows: $m_2 = \sqrt{\Delta m_{sun}^2 + m_1^2}$ and $m_3 = \sqrt{\Delta m_{atm}^2 + m_1^2}$. The values of $\Delta m_{sun}^2 = 7.58 \times 10^{-5}$ eV^2 and $\Delta m_{atm}^2 = 2.35 \times 10^{-3}$ eV^2 are the best-fit values at 1σ taken from [16].

After introduce these values of masses in Eq. (8), we evaluate the neutrino evolution Hamiltonian in matter, Eq. (15), calculating the new mass eigenvalues and diagonalizing it to obtain the new mixing matrix. It is important to notice that for each set (ϵ, m_1) we are going to have new elements of the mixing matrix and new mass eigenstates either in vacuum and in matter. Then we evaluate the probabilities using Eq. (17) and average them in the region of production. In Fig. 4, the survival probability, P_{ee}, is represented by the solid black curve. Conversion probabilities are represented

in the following way: P_{ea} ($a = \mu, \tau$) is the dotted red curve and P_{es} is the dashed blue curve.

In Fig. 5 we have plotted the probabilities for the CASE A for $\epsilon = 1.0 \times 10^{-9}$ and $m_1 = 0.003$ eV. Notation and representation of the curves are the same as in Fig. 4.

We notice, for example, for small ϵ, such as $\epsilon = 1.0 \times 10^{-9}$ in Fig. 5, that the quasi-Dirac situation mimics the standard one, since we do not see a significant conversion to the sterile neutrino flavor. So, when $\epsilon \to 0$, or simply to very small values, we approach the traditional solar neutrino solution. However, for higher ϵ, such as we saw in Fig. 4 ($\epsilon = 1 \times 10^{-7}$), conversion to sterile neutrinos can be significant for the entire neutrino spectrum. If we get an even higher ϵ, we will see an even larger oscillation pattern of P_{es}. This also happens for the other channels of oscillations ($\nu_e \to \nu_{\mu,\tau}$). That is because with a larger radiative correction, ϵ, we get $\Delta m_{ij}^2 L/(2E) \gg 1$. The phenomenological effect of m_1 is very similar. For large values of m_1, if we fix $\epsilon \neq 0$, we are going to have more oscillation if we compare to the situation with a smaller m_1.

One of the main sources of neutrinos, considering SNO and SK as experiments, is the ^{8}B. For energies above a few MeV, SNO and SK reveal that $P_{ee} \approx 0.3$ and also $P_{ea} \approx 0.7$. This is a very strong constraint. For energies below 1 MeV or so, the constraints come mainly from Borexino, Homestake, and the gallium experiments. Borexino imposes $P_{ee} \approx 0.51$. Then if we have larger values of P_{es}, P_{ee} must be higher to compensate the disappearance of active neutrinos (ν_μ or ν_τ) that would arrive in Earth detectors. For even lower neutrino energies, mainly of the pp chain, gallium experiments impose $P_{ee} \approx 0.5$. So any modification on P_{es} for the set of parameters ϵ, m_1 has to be compensated by P_{ee}, especially in the high energy part of the spectrum.

Fig. 4 Survival probabilities (P_{ee}—solid black curve) and conversion probabilities (P_{ea}—dotted red curve, and P_{es}—dashed blue curve) for the CASE A. All the curves correspond to $\epsilon = 5.0 \times 10^{-7}$ and $m_1 = 0.003$ eV. We do not show these probability curves for the CASE B, since their behavior is very similar and there are very small differences
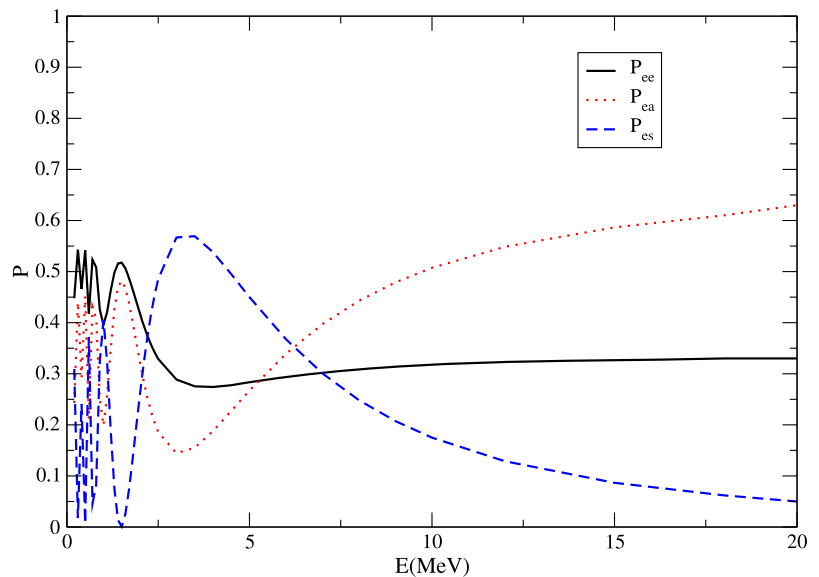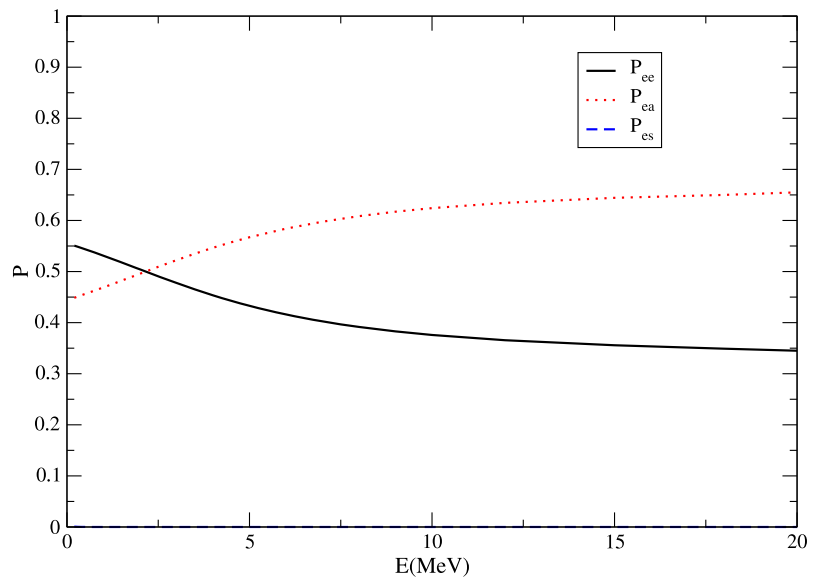
Fig. 5 Survival probabilities (P_{ee}—solid black curve) and conversion probabilities (P_{ea}—dotted red curve, and P_{es}—dashed blue curve) for the CASE A. All the curves correspond to $\epsilon = 1.0 \times 10^{-9}$ and $m_1 = 0.003$ eV. Similar results are obtained in CASE B

We do not show the plots for the CASE B, because the behavior and the pattern of the curves are very similar.

Next, we proceed with a χ^2 fit to the data. This will be used to constrain our model for both CASES A and B. We can define $\Delta\chi^2 = \chi^2(\epsilon, m_1) - \chi^2(\epsilon = 0)$, where $\chi^2(\epsilon = 0)$ is valid for any value of m_1, since $\epsilon = 0$ represents the standard situation and solar neutrino experiments are sensitive only to the mass squared difference and not to the absolute value of neutrino masses. For $\epsilon \neq 0$, we choose m_1 to vary from 0.001 eV to 1 eV. We remember that Katrin will impose a superior limit on neutrino mass of about 0.2 eV [48].

In Fig. 6, we present the allowed region for the CASE A and CASE B together. Below the curves are the allowed regions. The dashed curves are the 2σ allowed region for the parameters ϵ and m_1. The solid curves are the 3σ allowed

region. Thinner curves (black ones) represent the CASE A and thicker curves (red ones) represent the CASE B. In Fig. 7 we have the same analysis, now for m_4 values. We notice, as shown in both Fig. 6 and Fig. 7, that the value of the scale of m_1 is very similar to m_4, since $m_4 \sim m_2$, and $\Delta m_{21}^2 \sim \Delta m_{41}^2 \approx 7.5 \times 10^{-5}$ eV^2 for small ϵ. As the radiative correction (ϵ) grows, m_1 (m_4) has to diminish to maintain the χ^2. They have, in some sense, a compensatory behavior when considered together. We remember for CASE B that $\epsilon = \epsilon_\tau$ ($\epsilon' = \epsilon'_\tau$), and ϵ and ϵ' are related by Eq. (13).

In Fig. 6 and Fig. 7, we have plotted all the curves together to make evident the difference between CASE A and CASE B. We notice that there is a very small difference between these two approximations, which would be evidence that it is almost impossible to distinguish between them.

Fig. 6 Allowed regions for the parameters ϵ and m_1. Thinner curves (black curves) represent the CASE A. Thicker curves (red curves) represent the CASE B
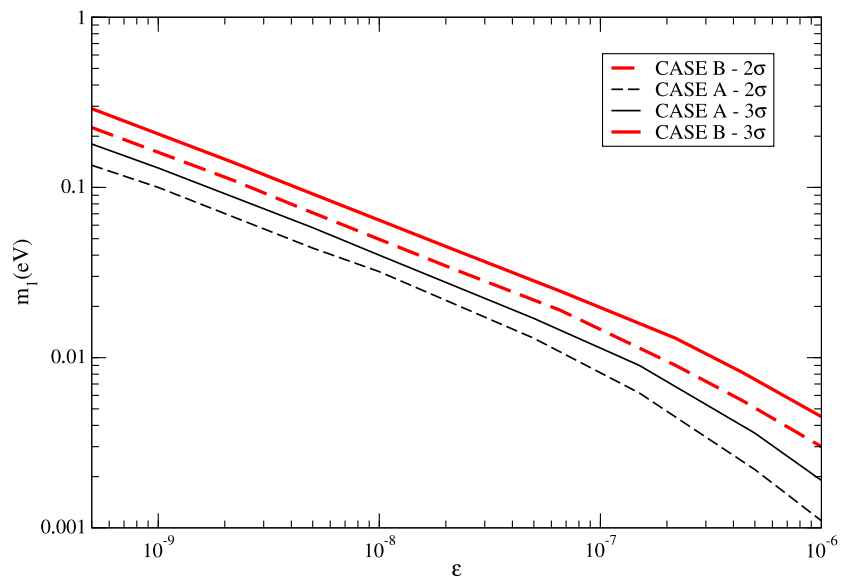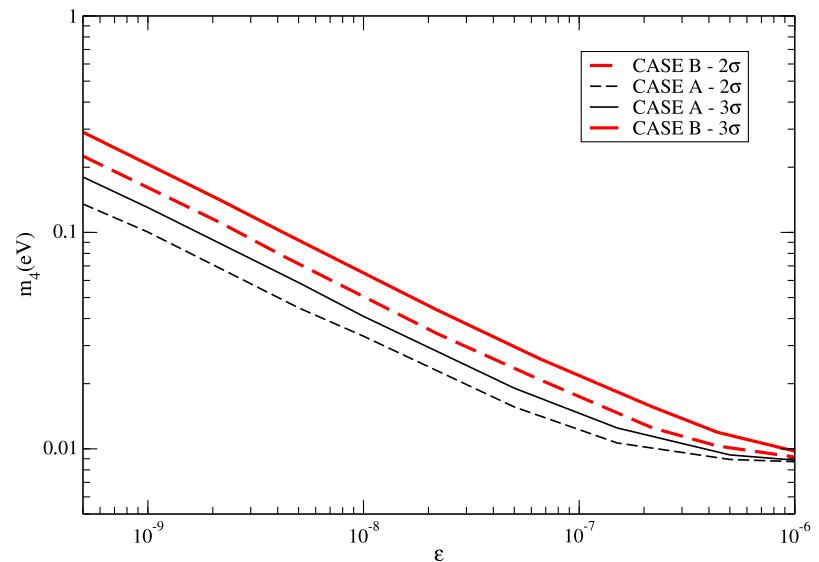
Fig. 7 Allowed regions for the parameters ϵ and m_4. *Thinner curves* (*black curves*) represent the CASE A. *Thicker curves* (*red curves*) represent the CASE B

Our results are similar to the ones found by de Gouvêa et al. [13]. They found in the $2+1$ case (two active neutrinos + one sterile) that $\epsilon < 2.0 \times 10^{-7}$ for 3σ and $\epsilon < 1.2 \times 10^{-7}$ for 2σ. Their model has only the ϵ parameter, however, our model possesses two parameters. Despite this fact, as we can see in Fig. 7, we also have found similar values of ϵ when 0.01 eV $< m_4 < 0.2$ eV at 2σ level. The important characteristic of the model, quasi-degeneracy with the m_2 state (Δm_{24}^2 much smaller than the other ones), is still maintained even for these m_4 values of masses. In both cases, the mixing matrix U after radiative corrections and solar neutrino data analysis remains the TBM one for all practical purposes, represented by Eq. (3).

5 Conclusions

In this paper we have analyzed the model with a quasi-Dirac neutrino put forward in Refs. [5, 12] using the solar neutrino data. This is possible because when radiative corrections are included in the neutrino mass matrix the oscillation channel $\nu_e \to \nu_s$ is open. However, we have got the result that, even in this case, the quasi-Dirac neutrino remains, for all practical proposes, a Dirac one, i.e., $m_2 \approx m_4$. Our model has two parameters, the radiative correction ϵ and the input mass m_1, which is the small one considering, for simplicity, the normal hierarchy. We have found allowed regions, shown in Fig. 7, in which ϵ can vary approximately from 5×10^{-9} to 10^{-6} and the m_4 mass varying from 0.01 eV (0.01 eV) to 0.2 eV (0.3 eV) at 2σ (3σ) level. Using Eq. (12), this implies 10^{12} GeV$^4 \lesssim k_x k_y \langle \phi_x \rangle \langle \phi_y \rangle \lesssim 10^{14}$ GeV^4, which means that we have four mass scales between ~ 1 TeV and ~ 3 TeV. The m_4 values are compatible with the most conservative limit of the sum of neutrino masses ($\sum_{m_\nu} < 1.3$ eV (95 %)) of WMAP-7 [24]. In Ref. [13], which describes a

$2+1$ model—two active neutrinos plus one sterile—it was obtained $\epsilon < (1.2, 2.0) \times 10^{-7}$ at two and three sigma level, respectively. Note that in our case the four masses belong to the interval with order of magnitude $\sim (10^{-3}$–$10^{-1})$ eV.

Summarizing, even with radiative corrections are considered, the mixing matrix in the lepton sector continues to be the tribimaximal one. It means that in these conditions the model cannot explain the disappearance of $\bar{\nu}_e$ observed by several experiments and, when interpreted in a three active neutrino scenario, it implies a non-zero θ_{13} [9–11]. Hence, the only way to obtain a realistic PMNS mixing matrix is by considering a non-diagonal charged lepton mass matrix as has been put forward in Ref. [12]. This will introduce contributions with crossed masses: $m_e m_\mu$, etc., but none of them are as important like the term proportional to m_τ^2. By doing this our results will not be significantly modified.

References

1. L. Wolfenstein, Nucl. Phys. B **186**, 147 (1981)
2. S.T. Petcov, Phys. Lett. B **110**, 245 (1982)
3. M. Doi, M. Kenmoku, T. Kotani, H. Nishiura, E. Takasugi, Prog. Theor. Phys. **70**, 1331 (1983)
4. J.W.F. Valle, Phys. Rev. D **27**, 1672 (1983)
5. A.C.B. Machado, V. Pleitez, Phys. Lett. B **698**, 128 (2011). arXiv:1008.4572 [hep-ph]
6. R. Allahverdi, B. Dutta, R.N. Mohapatra, Phys. Lett. B **695**, 181 (2011). arXiv:1008.1232 [hep-ph]
7. J. Barry, R.N. Mohapatra, W. Rodejohann, Phys. Rev. D **83**, 113012 (2011). arXiv:1012.1761 [hep-ph]

8. P.F. Harrison, D.H. Perkins, W.G. Scott, Phys. Lett. B **530**, 167 (2002). hep-ph/0202074

9. F.P. An et al. (DAYA-BAY Collaboration), Phys. Rev. Lett. **108**, 171803 (2012). arXiv:1203.1669 [hep-ex]

10. J.K. Ahn et al. (RENO Collaboration), Phys. Rev. Lett. **108**, 191802 (2012). arXiv:1204.0626 [hep-ex]

11. Y. Abe et al. (Double Chooz Collaboration), Phys. Rev. D **86**, 052008 (2012). arXiv:1207.6632 [hep-ex]

12. A.C.B. Machado, V. Pleitez, J. Phys. G, Nucl. Part. Phys. **40**, 035002 (2013). arXiv:1105.6064 [hep-ph]

13. A. de Gouvea, W.-C. Huang, J. Jenkins, Phys. Rev. D **80**, 073007 (2009). arXiv:0906.1611 [hep-ph]

14. G.L. Fogli, E. Lisi, A. Marrone, D. Montanino, A. Palazzo, A.M. Rotunno, Phys. Rev. D **86**, 013012 (2012). arXiv:1205.5254 [hep-ph]

15. D.V. Forero, M. Tortola, J.W.F. Valle, Phys. Rev. D **86**, 073012 (2012). arXiv:1205.4018 [hep-ph]

16. J. Beringer et al. (Particle Data Group Collaboration), Phys. Rev. D **86**, 010001 (2012)

17. K.N. Abazajian et al., arXiv:1204.5379

18. B. Kayser, arXiv:1207.2167 and references therein

19. A. Aguilar et al. (LSND Collaboration), Phys. Rev. D **64**, 112007 (2001). hep-ex/0104049

20. A.A. Aguilar-Arevalo et al. (MiniBooNE Collaboration), arXiv:1207.4809 [hep-ex]

21. T.A. Mueller, D. Lhuillier, M. Fallot, A. Letourneau, S. Cormon, M. Fechner, L. Giot, T. Lasserre et al., Phys. Rev. C **83**, 054615 (2011). arXiv:1101.2663 [hep-ex]

22. P. Huber, Phys. Rev. C **84**, 024617 (2011). Erratum-ibid. C **85**, 029901 (2012). arXiv:1106.0687 [hep-ph]

23. C. Giunti, M. Laveder, Phys. Rev. C **83**, 065504 (2011). arXiv:1006.3244 [hep-ph]

24. E. Komatsu et al. (WMAP Collaboration), Astrophys. J. Suppl. Ser. **192**, 18 (2011). arXiv:1001.4538 [astro-ph.CO]

25. B.T. Cleveland, T. Daily, R. Davis Jr., J.R. Distel, K. Lande, C.K. Lee, P.S. Wildenhain, J. Ullman, Astrophys. J. **496**, 505 (1998)

26. W. Hampel et al. (GALLEX Collaboration), Phys. Lett. B **447**, 127 (1999)

27. J.N. Abdurashitov et al. (SAGE Collaboration), J. Exp. Theor. Phys. **95**, 181 (2002). [Zh. Eksp. Teor. Fiz. **122**, 211 (2002)]. astro-ph/0204245

28. Y. Fukuda et al. (Kamiokande Collaboration), Phys. Rev. Lett. **77**, 1683 (1996)

29. J. Hosaka et al. (Super-Kamiokande Collaboration), Phys. Rev. D **73**, 112001 (2006). hep-ex/0508053

30. J. Boger et al. (SNO Collaboration), Nucl. Instrum. Methods Phys. Res., Sect. A, Accel. Spectrom. Detect. Assoc. Equip. **449**, 172 (2000). nucl-ex/9910016

31. G. Alimonti et al. (Borexino Collaboration), Nucl. Instrum. Methods Phys. Res., Sect. A, Accel. Spectrom. Detect. Assoc. Equip. **600**, 568 (2009). arXiv:0806.2400 [physics.ins-det]

32. M.C. Gonzalez-Garcia, M. Maltoni, Phys. Rep. **460**, 1 (2008). arXiv:0704.1800 [hep-ph]

33. V. Antonelli, L. Miramonti, C. Pena-Garay, A. Serenelli, Adv. High Energy Phys. **2013**, 351926 (2013). arXiv:1208.1356 [hep-ex]

34. W.C. Haxton, R.G. Hamish Robertson, A.M. Serenelli, arXiv:1208.5723 [astro-ph.SR]

35. G. Bellini, J. Benziger, D. Bick, S. Bonetti, G. Bonfini, M. Buizza Avanzini, B. Caccianiga, L. Cadonati et al., Phys. Rev. Lett. **107**, 141302 (2011). arXiv:1104.1816 [hep-ex]

36. G. Bellini et al. (Borexino Collaboration), Phys. Rev. Lett. **108**, 051302 (2012). arXiv:1110.3230 [hep-ex]

37. Q.R. Ahmad et al. (SNO Collaboration), Phys. Rev. Lett. **89**, 011301 (2002). nucl-ex/0204008

38. S.N. Ahmed et al. (SNO Collaboration), Phys. Rev. Lett. **92**, 181301 (2004). nucl-ex/0309004

39. B. Aharmim et al. (SNO Collaboration), Phys. Rev. C **72**, 055502 (2005). nucl-ex/0502021

40. M. Altmann et al. (GNO Collaboration), Phys. Lett. B **616**, 174 (2005). hep-ex/0504037

41. J.N. Bahcall, A.M. Serenelli, S. Basu, Astrophys. J. Suppl. Ser. **165**, 400 (2006). Data and other relevant information can be found in http://www.sns.ias.edu/~jnb/. astro-ph/0511337

42. J.N. Bahcall, A.M. Serenelli, S. Basu, Astrophys. J. **621**, L85 (2005). astro-ph/0412440

43. C. Giunti, C.W. Kim, *Fundamentals of Neutrino Physics and Astrophysics* (Oxford University Press, Oxford, 2007), 710 p.

44. L. Wolfenstein, Phys. Rev. D **17**, 2369 (1978)

45. S.P. Mikheev, A.Y. Smirnov, Sov. J. Nucl. Phys. **42**, 913 (1985). [Yad. Fiz. **42**, 1441 (1985)]

46. T.-K. Kuo, J.T. Pantaleone, Rev. Mod. Phys. **61**, 937 (1989)

47. M. Cirelli, G. Marandella, A. Strumia, F. Vissani, Nucl. Phys. B **708**, 215 (2005). hep-ph/0403158

48. E.W. Otten, C. Weinheimer, Rep. Prog. Phys. **71**, 086201 (2008). arXiv:0909.2104 [hep-ex]